Supporting Information

Improving uncertainty estimation in urban hydrological modeling by statistically describing bias

Hydrology and Earth System Sciences

D. Del Giudice, M. Honti, A. Scheidegger, C. Albert, P. Reichert, and J. Rieckermann

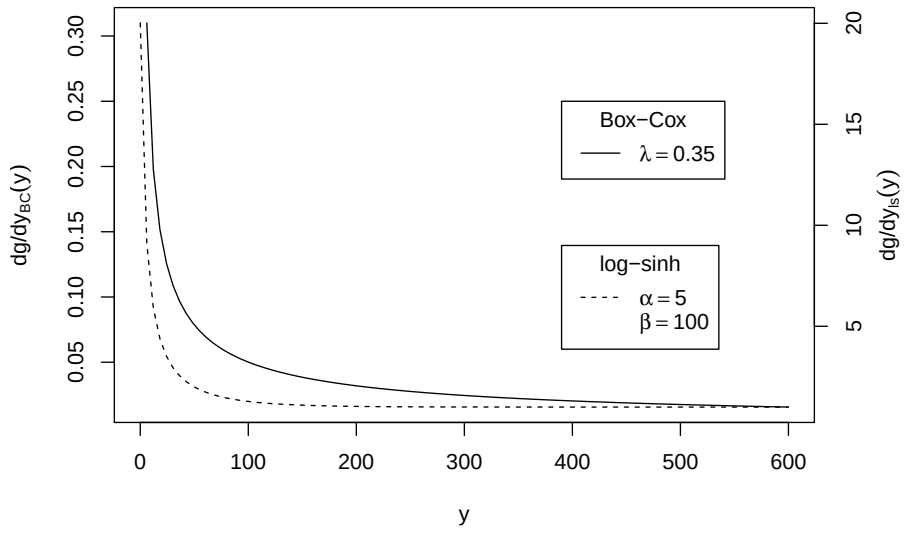

Figure S1: Behavior of the Box-Cox (solid line) and log-sinh (dashed line) transformation derivative as a function of the output variable (e.g. discharge in l/s) with parameters used in this study.

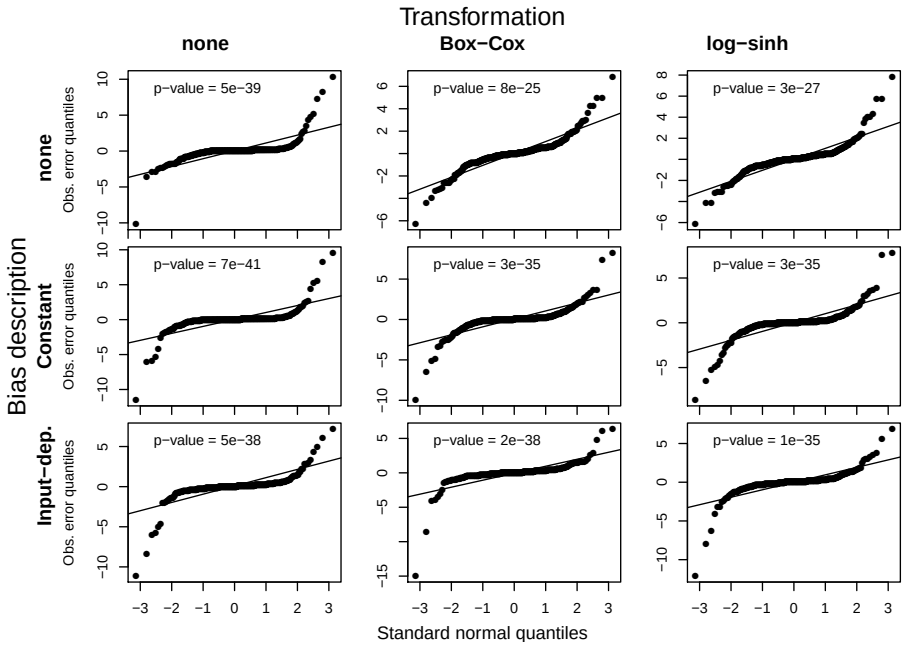

Figure S2: Quantile-Quantile plots for median of **E** (frequentist part of the residuals due to random measurement errors) in the calibration period of 22/23 July.

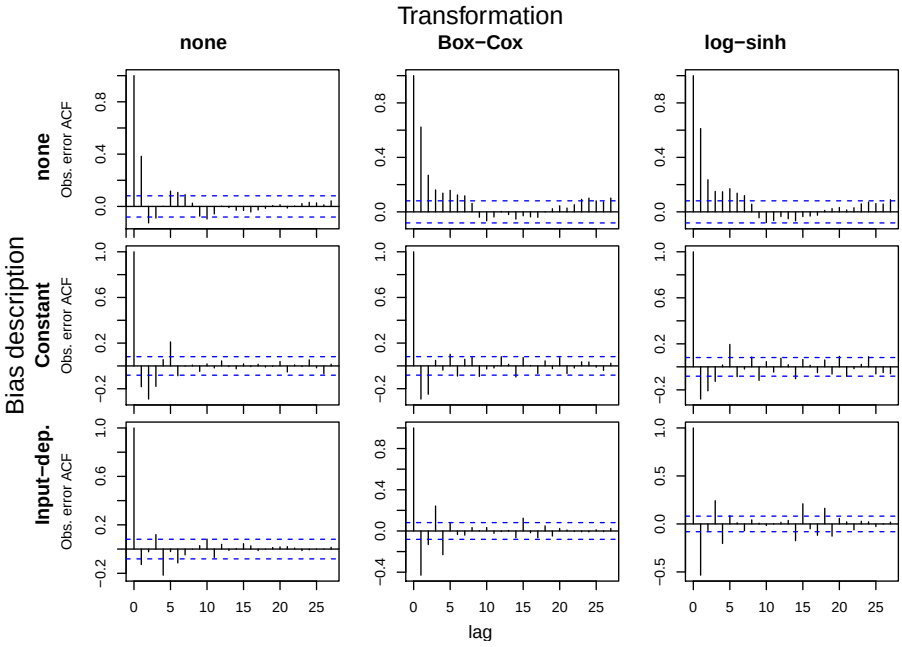

Figure S3: Autocorrelation Function plots for median of **E** (frequentist part of the residuals due to random measurement errors) in the calibration period of 22/23 July.

Table S1: Hydrodynamic model and error model calibration parameters ($\boldsymbol{\theta}, \boldsymbol{\psi}$). The notation for prior distributions is: LN(μ, σ): lognormal, TN(μ, σ, a_1, a_2): truncated normal, Exp(λ^{-1}): exponential. The symbol meaning is: μ: expected value, σ: standard deviation, a_1: lower limit, a_2: upper limit, λ: rate.

Name	Description	Units	Prior
Immeabilitas	Imperviousness in %	[-]	LN(38.2,3.82)
Amplitudo	Characteristic Width of the overland flow path	m	LN(900,90)
Affluentia	Baseline Inflow	l/s	LN(3,0.3)
Acclivitas	Catchment Slope in %	[-]	LN(6,0.6)
Longitudo	Conduit Length	m	LN(250,25)
corrlen	Correlation Length of **B** (τ)	min	LN(5,3)
sd.Eps_Q	Standard Deviation of **E** (σ_E)	g(l/s)	LN(2·$\left(\frac{\mathrm{d}g}{\mathrm{d}y}\right)_{100}$,.2·$\left(\frac{\mathrm{d}g}{\mathrm{d}y}\right)_{100}$)
sd.B_Q	Standard Deviation of **B** ($\sigma_{B_{ct}}$)	g(l/s)	TN(0,20·$\left(\frac{\mathrm{d}g}{\mathrm{d}y}\right)_{100}$,0,$10^6$)
ks_Q	Proportionality Constant between precipitation and uncertainty increase (κ)	g(l/s)·(s/mm)	TN($\frac{g(0)}{0.014}$,($\frac{g(390)-g(0)}{0.014}$),$\frac{g(0)}{0.014}$,$10^6$)
Delta	Delay between precipitation and uncertainty increase (δ)	[-]	Exp(3)

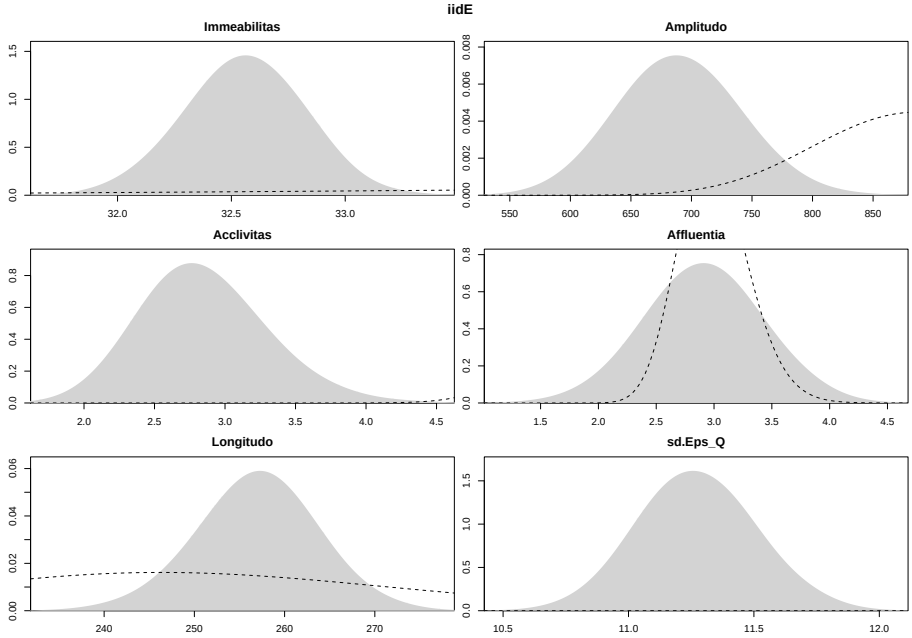

Figure S4: Prior (dashed lines) and posterior marginal distributions (gray areas) for $\boldsymbol{\theta}, \boldsymbol{\psi}$ (deterministic model and error model parameters) with the iid untransformed error description. Parameters are described in Tab S1.

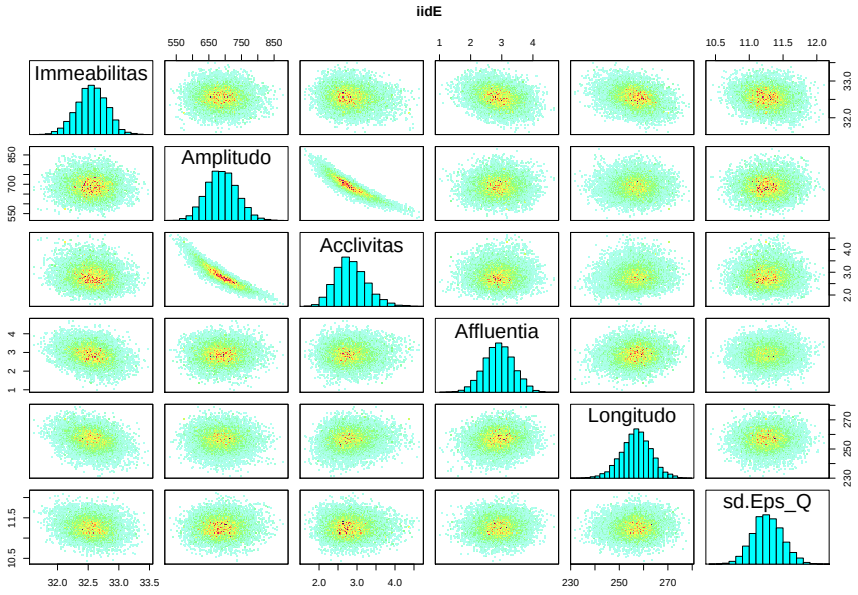

Figure S5: Pairwise scatterplot of posterior marginal distributions for $\boldsymbol{\theta}, \boldsymbol{\psi}$ (deterministic model and error model parameters) with the iid untransformed error description. Parameters are described in Tab S1.

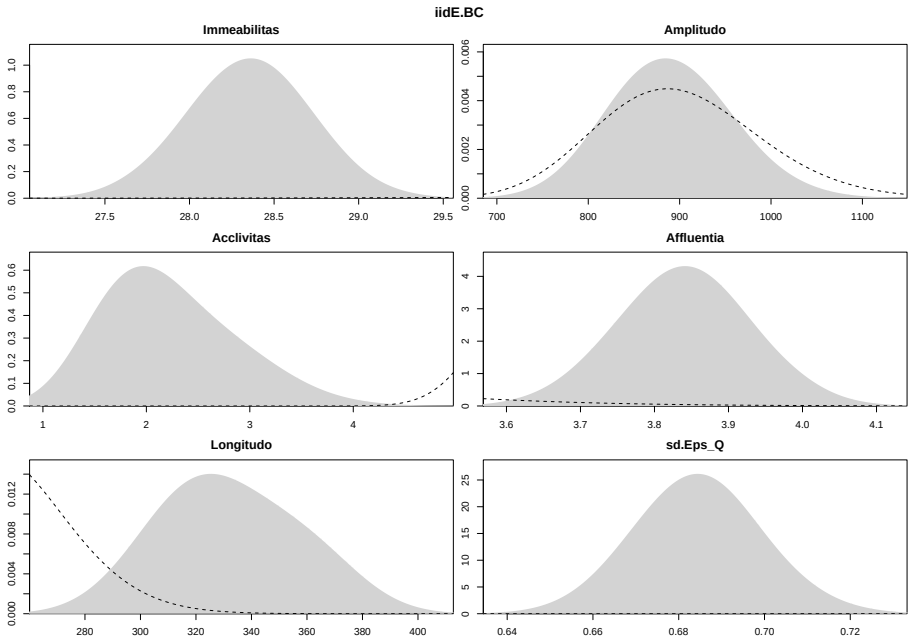

Figure S6: Prior (dashed lines) and posterior marginal distributions (gray areas) for $\boldsymbol{\theta}, \boldsymbol{\psi}$ (deterministic model and error model parameters) with the iid Box-Cox transformed error description. Parameters are described in Tab S1.

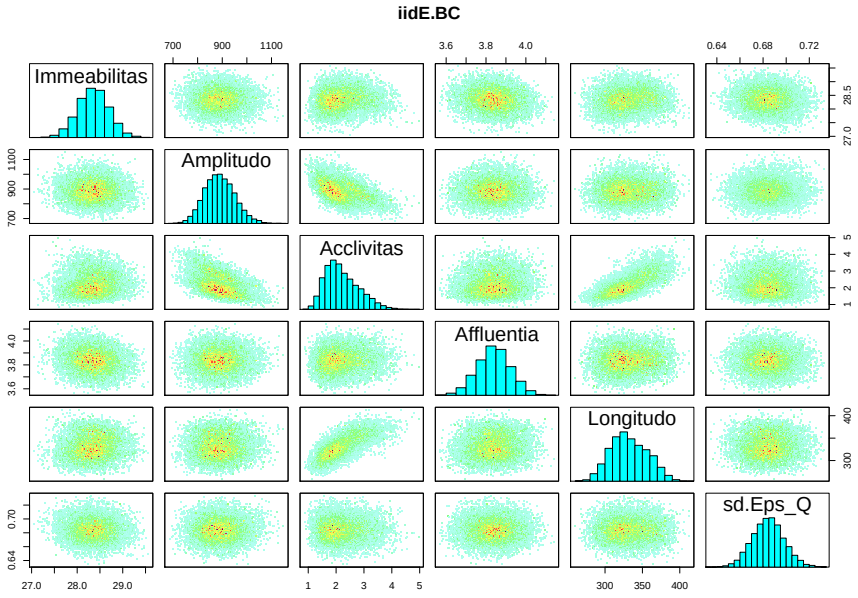

Figure S7: Pairwise scatterplot of posterior marginal distributions for $\boldsymbol{\theta}, \boldsymbol{\psi}$ (deterministic model and error model parameters) with the iid Box-Cox transformed error description. Parameters are described in Tab S1.

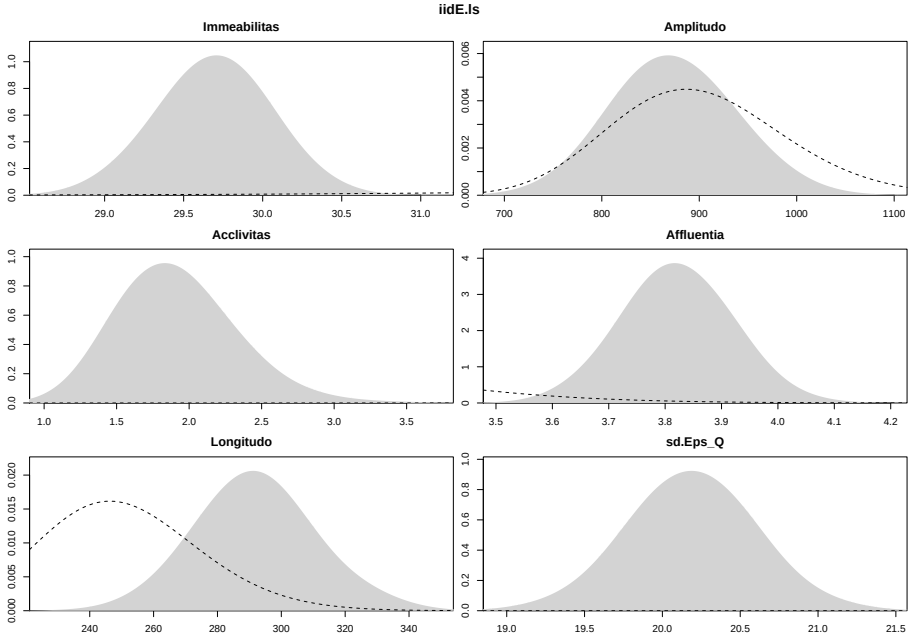

Figure S8: Prior (dashed lines) and posterior marginal distributions (gray areas) for $\boldsymbol{\theta}, \boldsymbol{\psi}$ (deterministic model and error model parameters) with the iid log-sinh transformed error description. Parameters are described in Tab S1.

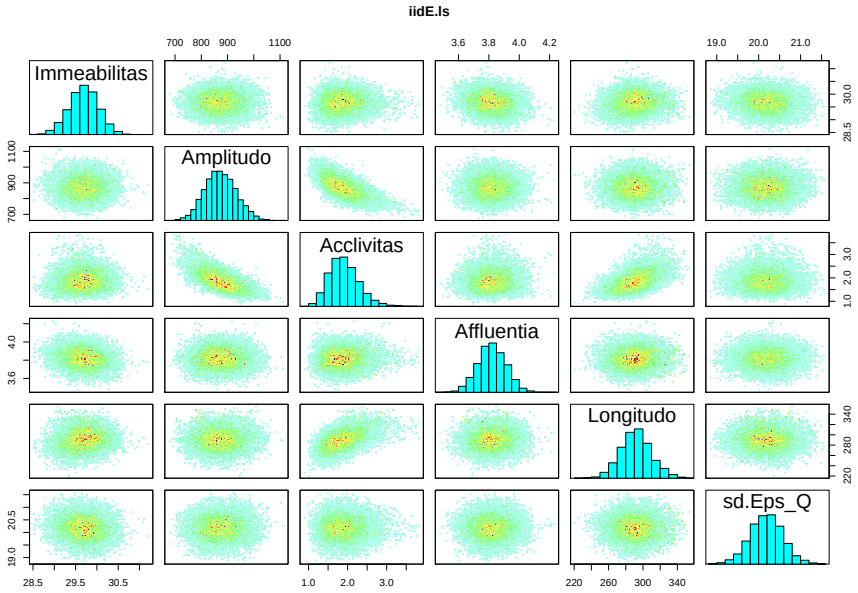

Figure S9: Pairwise scatterplot of posterior marginal distributions for $\boldsymbol{\theta}, \boldsymbol{\psi}$ (deterministic model and error model parameters) with the iid log-sinh transformed error description. Parameters are described in Tab S1.

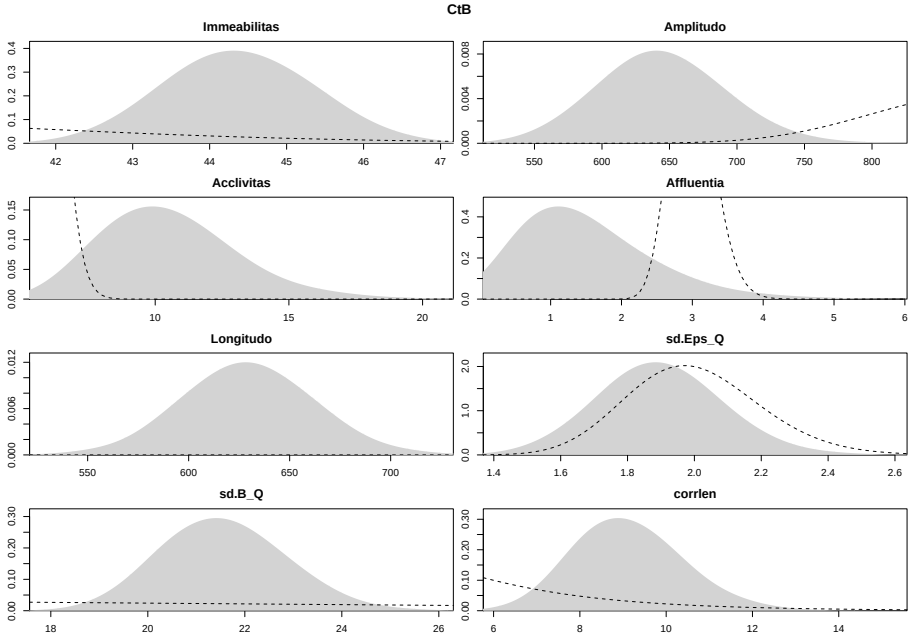

Figure S10: Prior (dashed lines) and posterior marginal distributions (gray areas) for $\boldsymbol{\theta}, \boldsymbol{\psi}$ (deterministic model and error model parameters) with the constant untransformed bias description. Parameters are described in Tab S1.

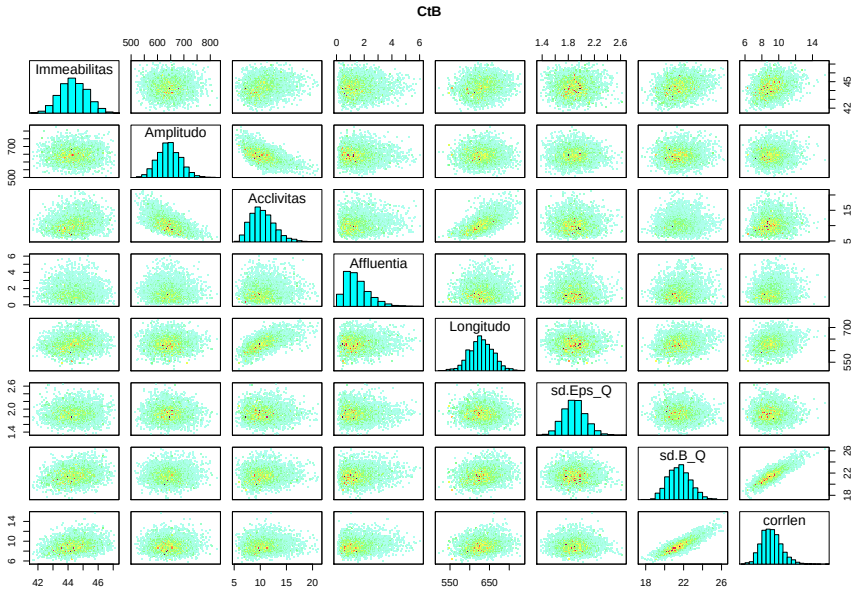

Figure S11: Pairwise scatterplot of posterior marginal distributions for $\boldsymbol{\theta}, \boldsymbol{\psi}$ (deterministic model and error model parameters) with the constant untransformed bias description. Parameters are described in Tab S1.

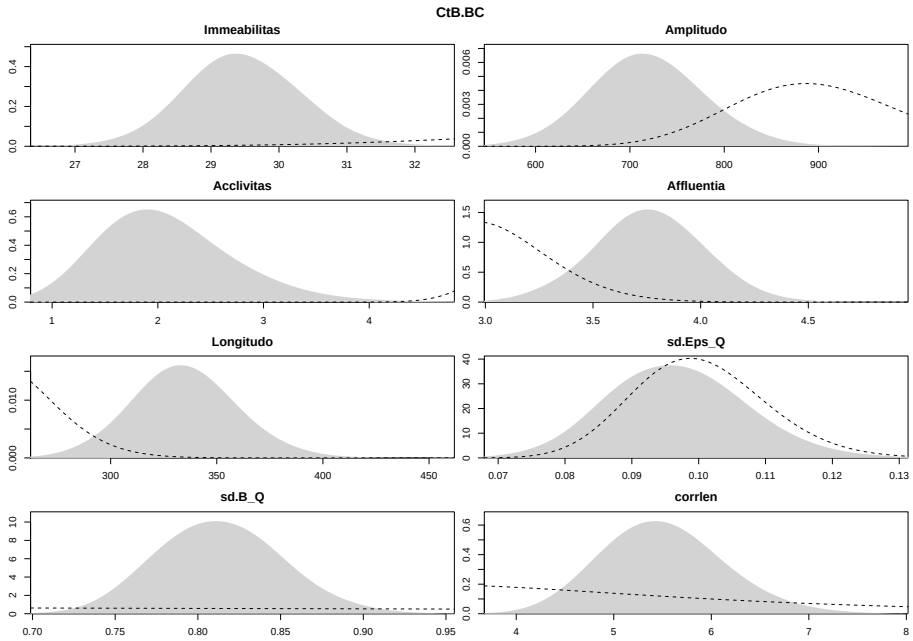

Figure S12: Prior (dashed lines) and posterior marginal distributions (gray areas) for $\boldsymbol{\theta}, \boldsymbol{\psi}$ (deterministic model and error model parameters) with the constant Box-Cox transformed bias description. Parameters are described in Tab S1.

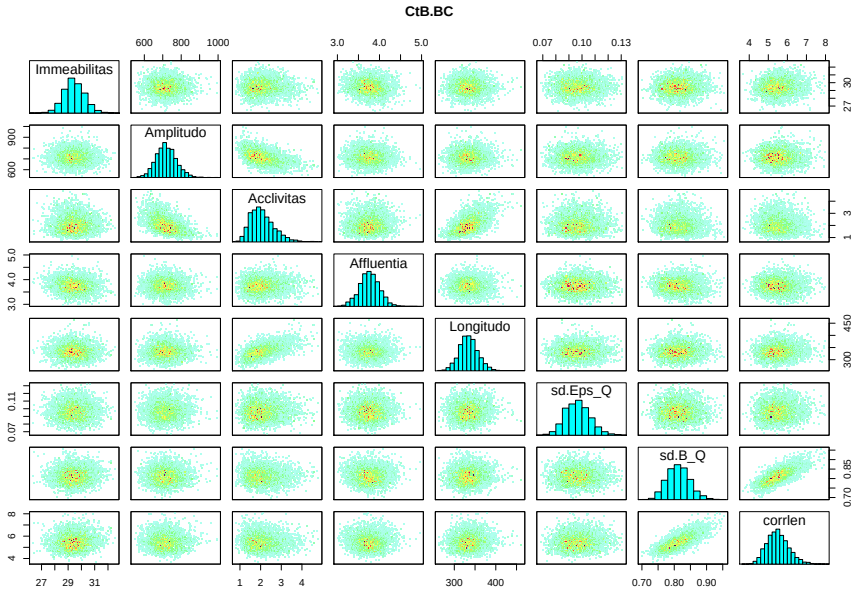

Figure S13: Pairwise scatterplot of posterior marginal distributions for $\boldsymbol{\theta}, \boldsymbol{\psi}$ (deterministic model and error model parameters) with the constant Box-Cox transformed bias description. Parameters are described in Tab S1.

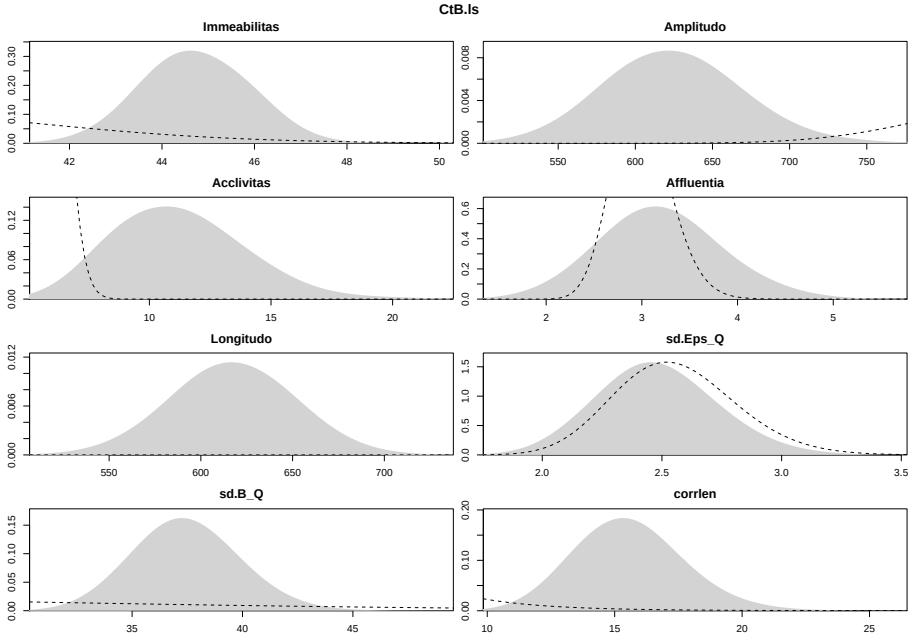

Figure S14: Prior (dashed lines) and posterior marginal distributions (gray areas) for $\boldsymbol{\theta}, \boldsymbol{\psi}$ (deterministic model and error model parameters) with the constant log-sinh transformed bias description. Parameters are described in Tab S1.

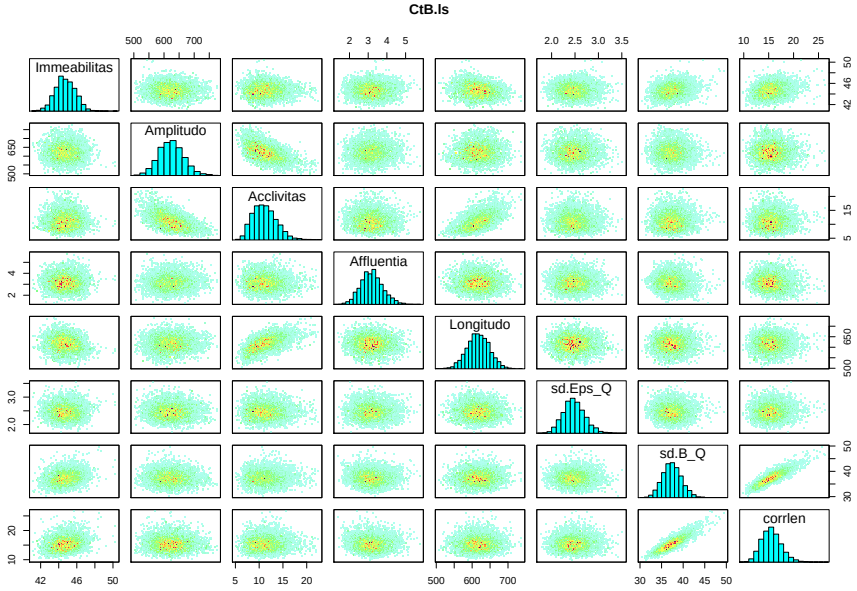

Figure S15: Pairwise scatterplot of posterior marginal distributions for $\boldsymbol{\theta}, \boldsymbol{\psi}$ (deterministic model and error model parameters) with the constant log-sinh transformed bias description. Parameters are described in Tab S1.

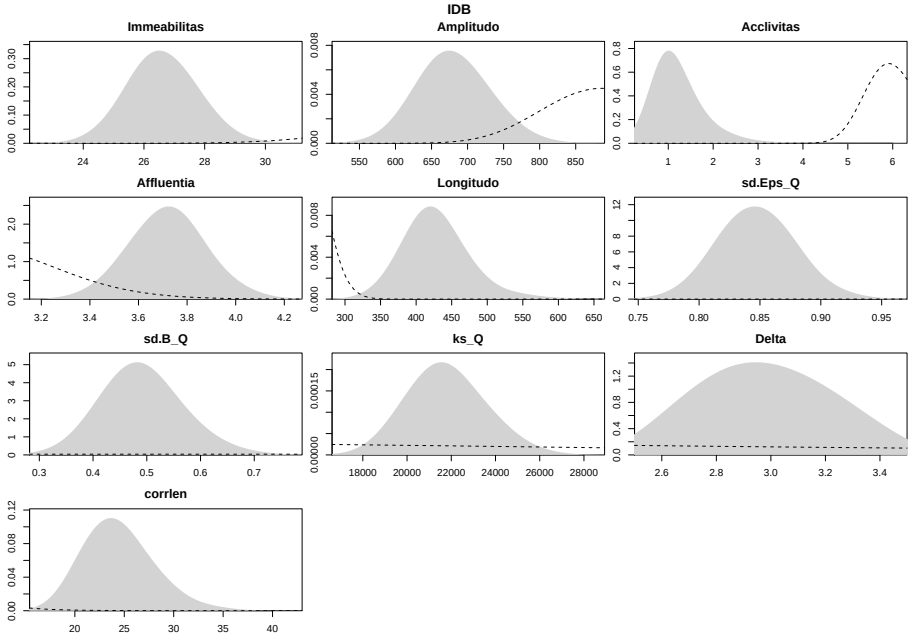

Figure S16: Prior (dashed lines) and posterior marginal distributions (gray areas) for $\boldsymbol{\theta}, \boldsymbol{\psi}$ (deterministic model and error model parameters) with the input-dependent untransformed bias description. Parameters are described in Tab S1.

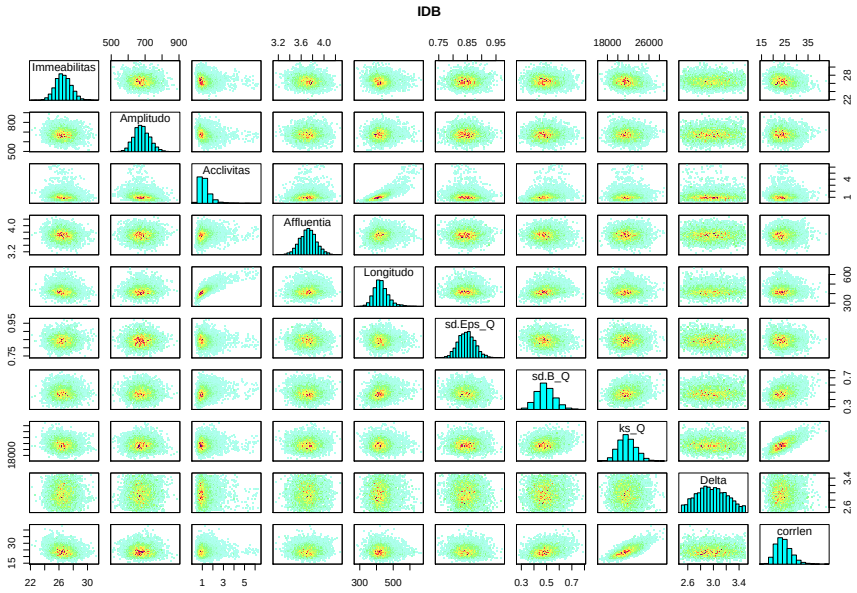

Figure S17: Pairwise scatterplot of posterior marginal distributions for $\boldsymbol{\theta}, \boldsymbol{\psi}$ (deterministic model and error model parameters) with the input-dependent untransformed bias description. Parameters are described in Tab S1.

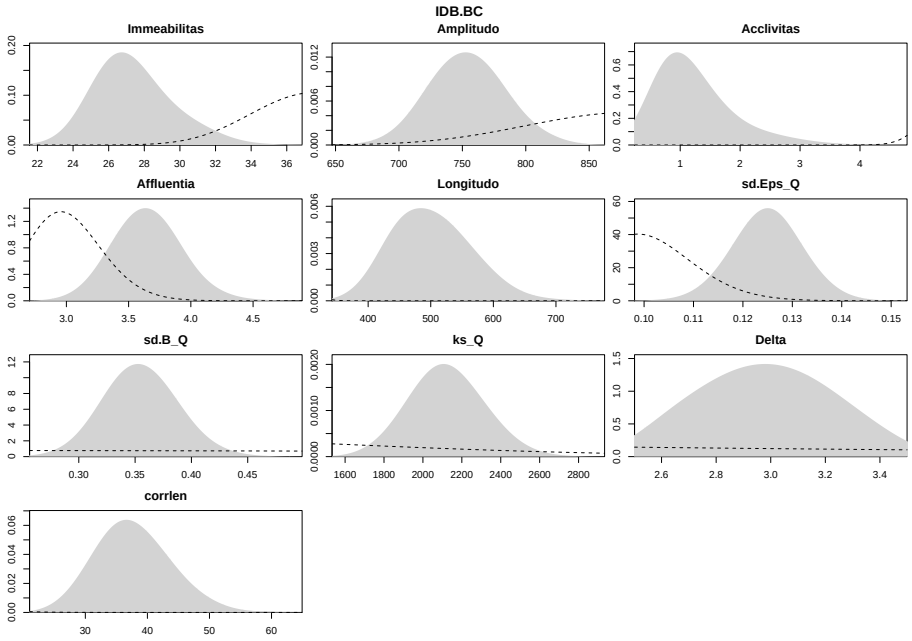

Figure S18: Prior (dashed lines) and posterior marginal distributions (gray areas) for $\boldsymbol{\theta}, \boldsymbol{\psi}$ (deterministic model and error model parameters) with the input-dependent Box-Cox transformed bias description. Parameters are described in Tab S1.

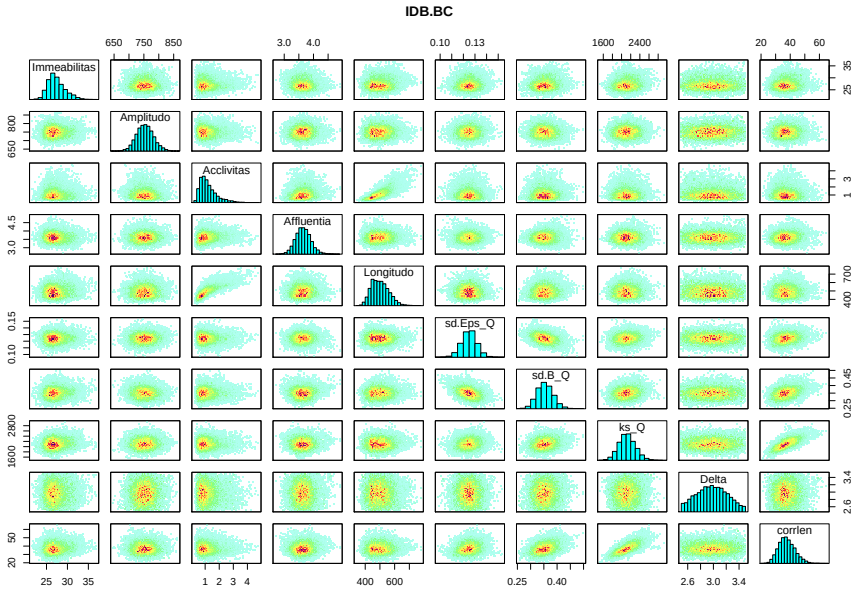

Figure S19: Pairwise scatterplot of posterior marginal distributions for $\boldsymbol{\theta}, \boldsymbol{\psi}$ (deterministic model and error model parameters) with the input-dependent Box-Cox transformed bias description. Parameters are described in Tab S1.

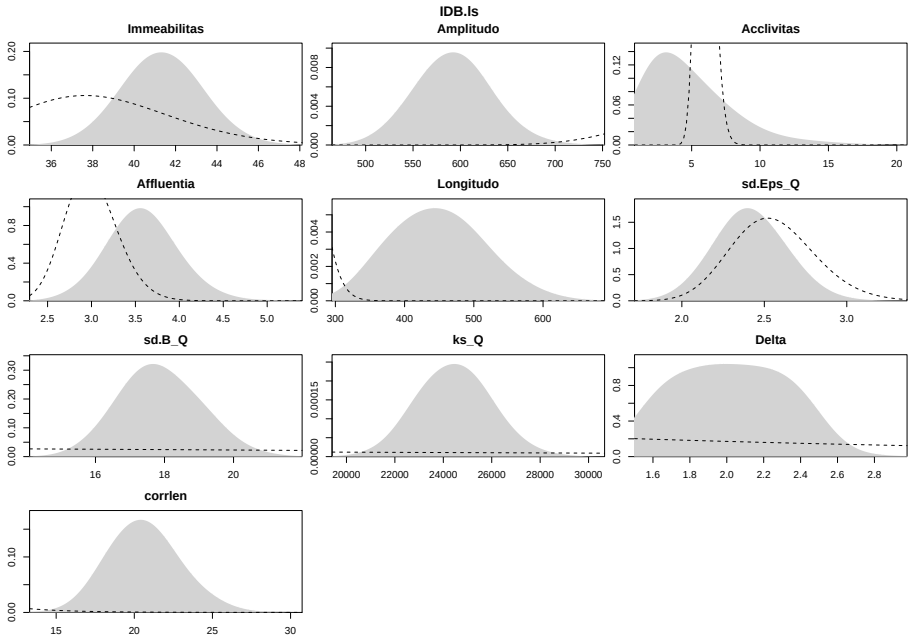

Figure S20: Prior (dashed lines) and posterior marginal distributions (gray areas) for $\boldsymbol{\theta}, \boldsymbol{\psi}$ (deterministic model and error model parameters) with the input-dependent log-sinh transformed bias description. Parameters are described in Tab S1.

Figure S21: Pairwise scatterplot of posterior marginal distributions for $\boldsymbol{\theta}, \boldsymbol{\psi}$ (deterministic model and error model parameters) with the input-dependent log-sinh transformed bias description. Parameters are described in Tab S1.

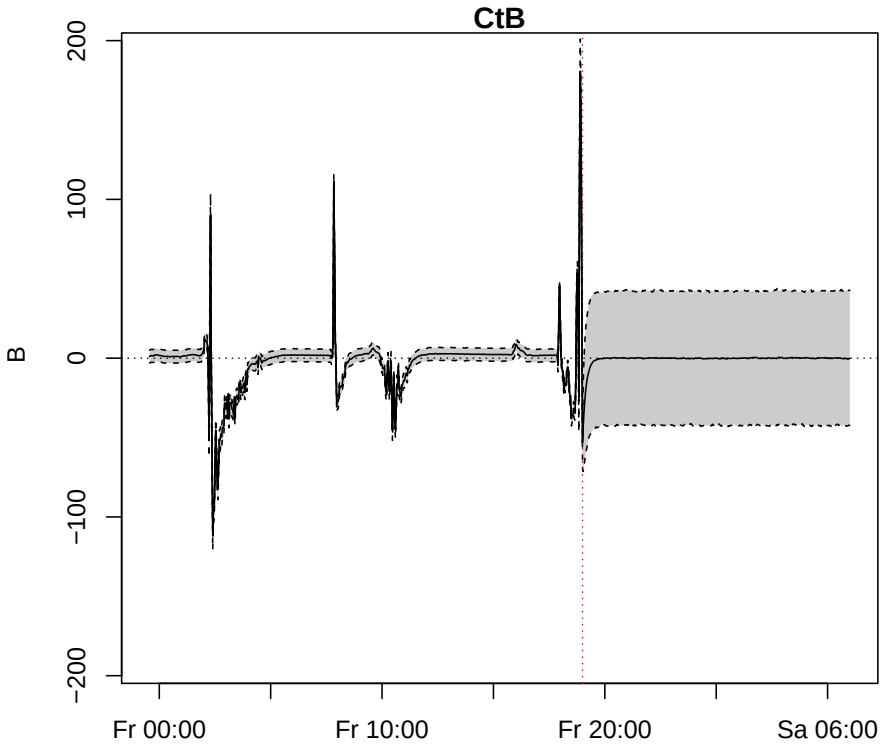

Figure S22: 95% credibility intervals (gray area bounded by dashed lines) and median (solid line) of the bias for part of the calibration (left) and the full validation period (right) obtained with the constant untransformed bias description. The ordinate axis is in transformed flow units. Note that here we do not display the bias-correction but the actual model bias $-\big(\tilde{\mathbf{Y}}_o(\mathbf{x},\boldsymbol{\theta},\boldsymbol{\psi}) - \tilde{\mathbf{y}}_M(\mathbf{x},\boldsymbol{\theta}) - \mathbf{E}(\boldsymbol{\psi})\big)$.

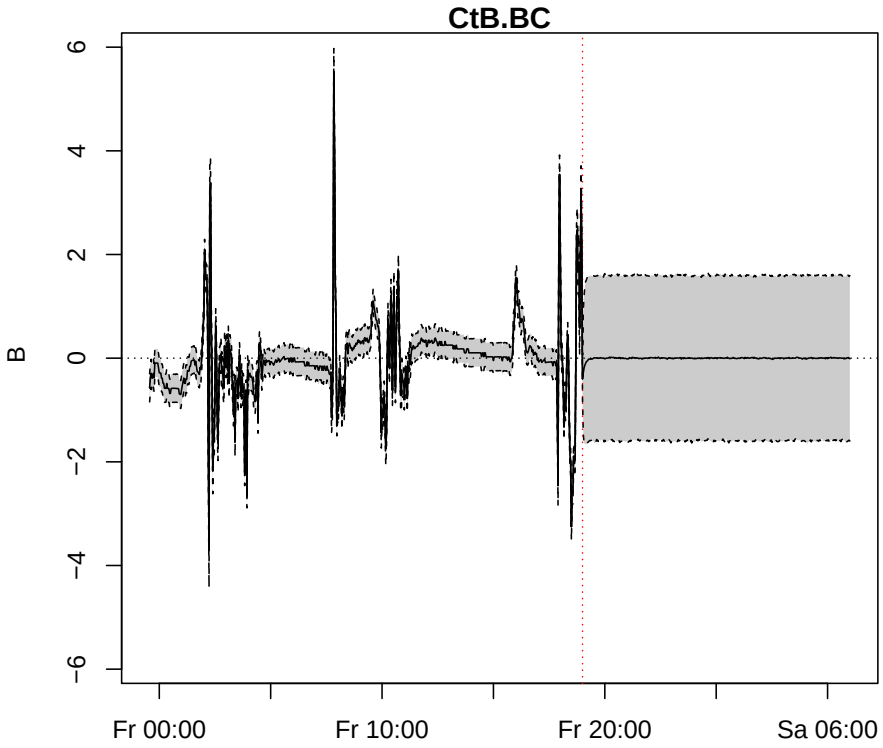

Figure S23: 95% credibility intervals (gray area bounded by dashed lines) and median (solid line) of the bias for part of the calibration (left) and the full validation period (right) obtained with the constant Box-Cox transformed bias description. The ordinate axis is in transformed flow units. Note that here we do not display the bias-correction but the actual model bias $-\big(\tilde{\mathbf{Y}}_o(\mathbf{x},\boldsymbol{\theta},\boldsymbol{\psi}) - \tilde{\mathbf{y}}_M(\mathbf{x},\boldsymbol{\theta}) - \mathbf{E}(\boldsymbol{\psi})\big)$.

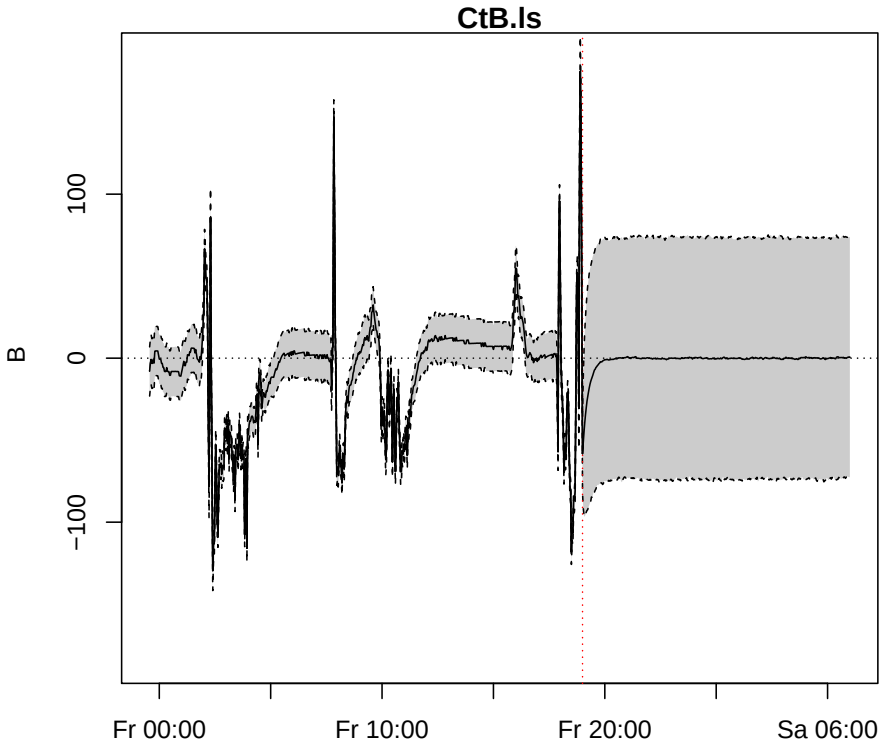

Figure S24: 95% credibility intervals (gray area bounded by dashed lines) and median (solid line) of the bias for part of the calibration (left) and the full validation period (right) obtained with the constant log-sinh transformed bias description. The ordinate axis is in transformed flow units. Note that here we do not display the bias-correction but the actual model bias $-\big(\tilde{\mathbf{Y}}_o(\mathbf{x},\boldsymbol{\theta},\boldsymbol{\psi}) - \tilde{\mathbf{y}}_M(\mathbf{x},\boldsymbol{\theta}) - \mathbf{E}(\boldsymbol{\psi})\big)$.

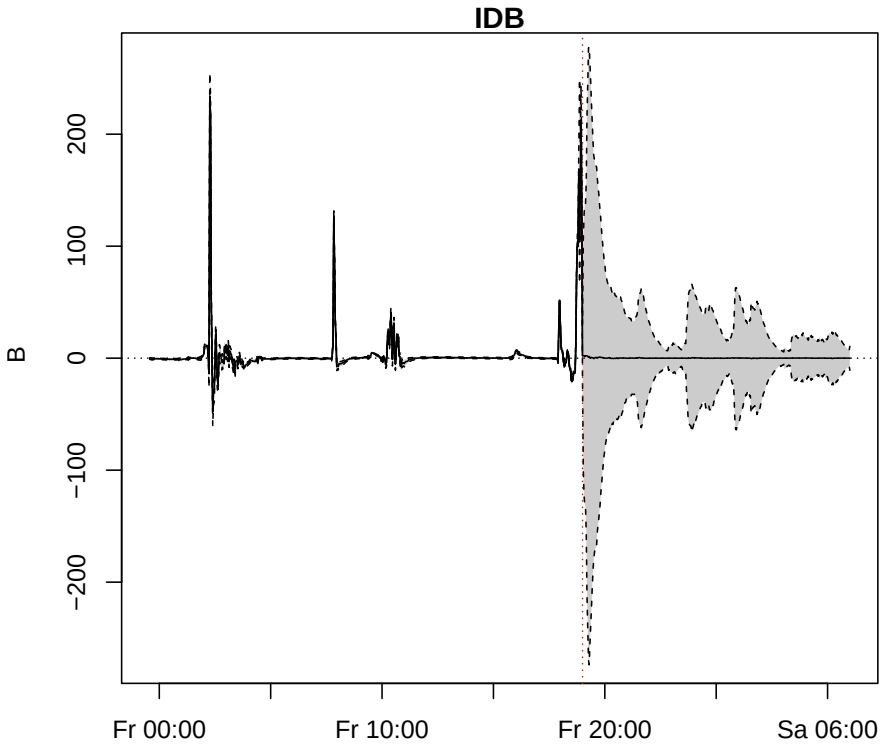

Figure S25: 95% credibility intervals (gray area bounded by dashed lines) and median (solid line) of the bias for part of the calibration (left) and the full validation period (right) obtained with the input-dependent untransformed bias description. The ordinate axis is in transformed flow units. Note that here we do not display the bias-correction but the actual model bias $-\big(\tilde{\mathbf{Y}}_o(\mathbf{x},\boldsymbol{\theta},\boldsymbol{\psi}) - \tilde{\mathbf{y}}_M(\mathbf{x},\boldsymbol{\theta}) - \mathbf{E}(\boldsymbol{\psi})\big)$.

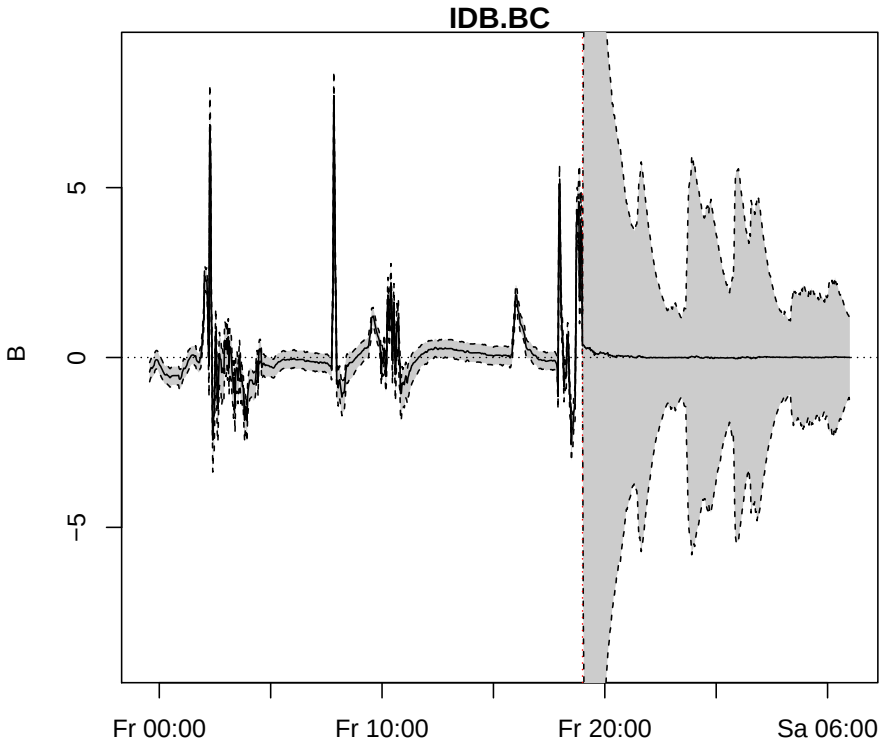

Figure S26: 95% credibility intervals (gray area bounded by dashed lines) and median (solid line) of the bias for part of the calibration (left) and the full validation period (right) obtained with the input-dependent Box-Cox transformed bias description. The ordinate axis is in transformed flow units. Note that here we do not display the bias-correction but the actual model bias $-\big(\tilde{\mathbf{Y}}_o(\mathbf{x},\boldsymbol{\theta},\boldsymbol{\psi}) - \tilde{\mathbf{y}}_M(\mathbf{x},\boldsymbol{\theta}) - \mathbf{E}(\boldsymbol{\psi})\big)$.

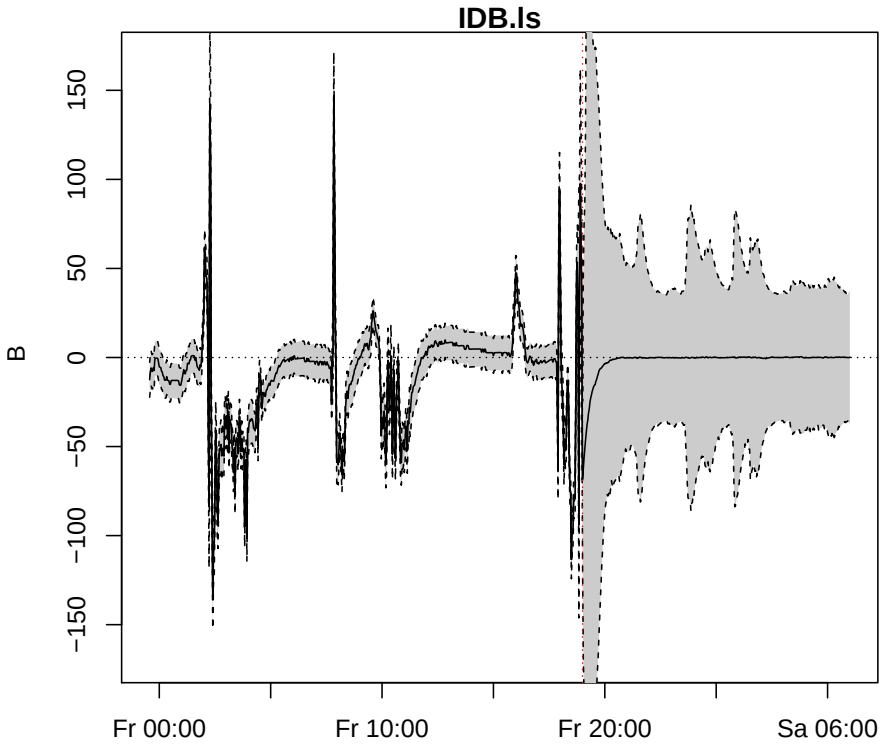

Figure S27: 95% credibility intervalis (gray area bounded by dashed lines) and median (solid line) of the bias for part of the calibration (left) and the full validation period (right) obtained with the input-dependent log-sinh transformed bias description. The ordinate axis is in transformed flow units. Note that here we do not display the bias-correction but the actual model bias $-\big(\tilde{\mathbf{Y}}_o(\mathbf{x},\boldsymbol{\theta},\boldsymbol{\psi}) - \tilde{\mathbf{y}}_M(\mathbf{x},\boldsymbol{\theta}) - \mathbf{E}(\boldsymbol{\psi})\big)$.

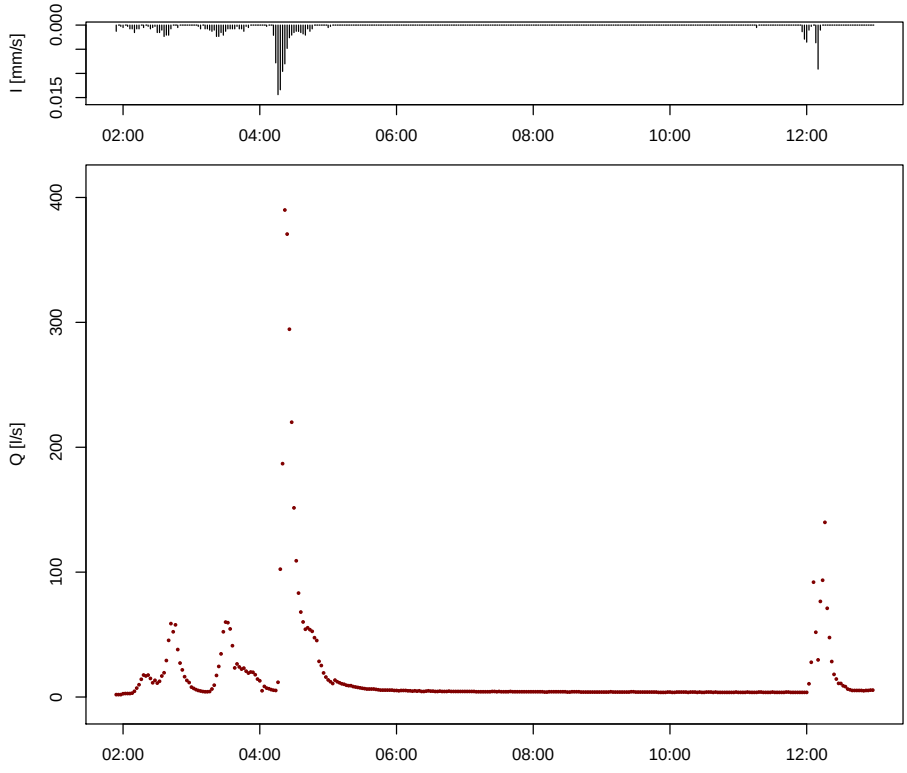

Figure S28: Monitoring data in the calibration period of 27 August.

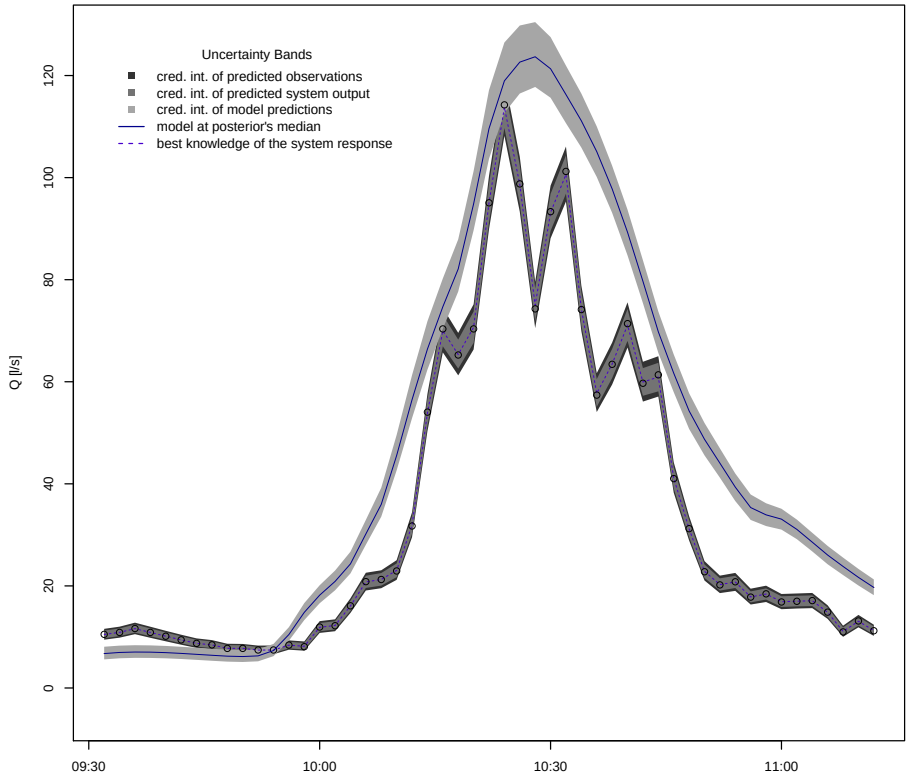

Figure S29: Magnified view of the runoff predictions for part of the calibration period with the constant bias model and log-sinh transformation. The observed hydrograph is represented by circles. The 95% credible intervals are interpreted as follows: parametric uncertainty due to $\vec{y}_{\mathrm{M}}$ (light gray), parametric plus input and structural uncertainty due to $g^{-1}(\tilde{\vec{y}}_{\mathrm{M}} + \vec{B}_{\mathrm{M}})$ (intermediate), total uncertainty due to $g^{-1}(\tilde{\vec{y}}_{\mathrm{M}} + \vec{B}_{\mathrm{M}} + \vec{E})$ (dark gray). The prediction intervals for the system output and the observations are almost indistinguishable and therefore only the intermediate gray band is visible at this scale.

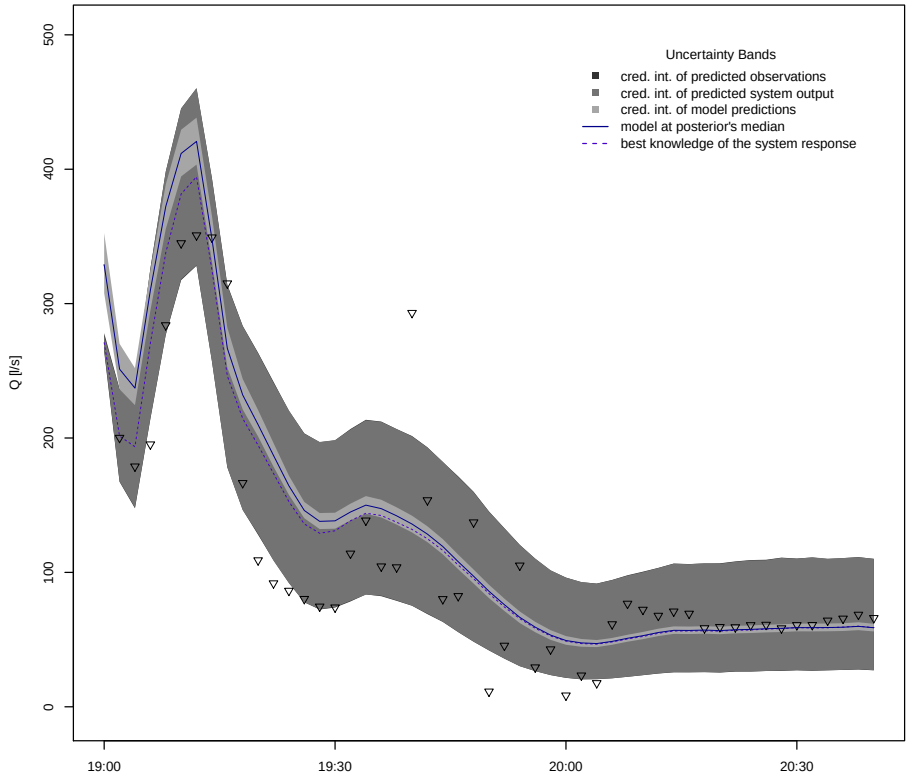

Figure S30: Magnified view of the runoff predictions for part of the validation period with the constant bias model and log-sinh transformation. The validation output data are represented by triangles. The 95% credible intervals are interpreted as follows: parametric uncertainty due to $\vec{y}_{\mathrm{M}}$ (light gray), parametric plus input and structural uncertainty due to $g^{-1}(\tilde{\vec{y}}_{\mathrm{M}} + \vec{B}_{\mathrm{M}})$ (intermediate), total uncertainty due to $g^{-1}(\tilde{\vec{y}}_{\mathrm{M}} + \vec{B}_{\mathrm{M}} + \vec{E})$ (dark gray). The prediction intervals for the system output and the observations are almost indistinguishable and therefore only the intermediate gray band is visible at this scale.